Research Article | Vol. 30, No. 19 / 12 Sep 2022 / Optics Express 34314
Optics EXPRESS

VO_2-based superposed Fabry-Perot multilayer film with a highly enhanced infrared emittance and emittance tunability for spacecraft thermal control

XIE BOWEI,[1,*] ZHANG WENJIE,[2] ZHAO JUNMING,[3] AND LIU LINHUA[2,4]

[1]Institute for Advanced Technology, Shandong University, Jinan 250061, China
[2]School of Energy and Power Engineering, Shandong University, Jinan 250061, China
[3]School of Energy Science and Engineering, Harbin Institute of Technology, Harbin 150001, China
[4]liulinhua@sdu.edu.cn
[*]xiebowei@sdu.edu.cn

Abstract: Thermal control coating for spacecraft based on thermochromic film attracts increasing interest due to their ability of self-adaptive emittance switch and less resource consuming compared with traditional thermal control coatings. However, practical applications of thermochromic film for spacecraft are constrained by the low infrared emittance at a high temperature and narrow emittance tunability. In this work, a thermochromic film with simple structure, nearly perfect infrared emission and large emittance tunability is proposed for the application of spacecraft thermal control. The thermochromic film is a VO_2-based superposed Fabry-Perot (FP) multilayer film, which is constructed by encapsulating three thin VO_2 layers in four lossless BaF_2 spacer on the Al substrate. The infrared emittance and emittance tunability of the superposed FP film is dramatically enhanced by the three superposed VO_2-BaF_2-Al FP resonances at wavelengths of 9, 15 and 20 μm, respectively. For VO_2 layers under metallic state, the spectral normal emittance of the superposed FP film is close to unity in the entire mid-infrared spectral range, while for VO_2 layers under dielectric state, the film is highly reflective. For the typical growth techniques of the VO_2 layers considered here, the emittance tunability of the superposed FP film can exceed 0.70 with total normal emittance larger than 0.91 at high temperature, simultaneously. The largest total normal emittance of the superposed FP film can reach 0.95 with emittance tunability of 0.78. In addition, the infrared emission and emittance tunability performances of the superposed FP film remain excellent for incident angles up to 60°. This work proposes a simple structure with highly enhanced infrared emittance and emittance tunability that outperforms the existing thermochromic films, which could accelerate the application of thermochromic films in the field of spacecraft thermal control.

1. Introduction

Spacecraft thermal management systems often cope with the violent alternation of high and low temperature working conditions in space, caused by the orbital eclipses, seasonal changes in solar intensity and sun angle variation, and dynamic internal thermal loads [1,2]. Thermal radiation is the only way for spacecraft to dissipate heat into outer space. However, the emittance of traditional thermal control coatings for spacecraft cannot be adjusted. A great amount of thermal compensation power and weight resources of the thermal control subsystem is needed for purpose of thermal control, which strongly restricts the life and reliability of the spacecraft [1–3]. By using an intelligent thermal control film which can switch its infrared emittance in orbit, the thermal compensation power and weight resources of thermal control subsystem can be reduced by more than 90 percent and 75 percent, respectively [3]. What's more, the primary benefit of

#464266 https://doi.org/10.1364/OE.464266
Journal © 2022 Received 18 May 2022; revised 25 Aug 2022; accepted 25 Aug 2022; published 6 Sep 2022

Optics EXPRESS

the intelligent thermal control film for crewed applications is to eliminate the need for dual loop thermal control architecture by preventing freezing of the radiator, and for robotic applications the benefit is to reduce the need for survival heaters [4]. Therefore, the development of intelligent thermal control films is critical for the rapidly increasing demand of spacecraft missions.

An intelligent thermal control film is mainly based on the far-field thermal radiation. Such films might be of three types: the thermochromic film [5,6], the electrochromic film [7,8] and the shutter regulation technology [9]. Most recently, a new principle of smart skin based on electric tuning of near-field radiative heat flux is proposed for spacecraft thermal control [10]. Among these technologies, the thermochromic film based on thermally driven phase change materials is the only scheme that can automatically switch its emittance without additional energy consumption, which shows great potential for the application of spacecraft thermal control. Typical thermally driven phase change materials include chalcogenides (such as $Ge_2Sb_2Te_5$) with amorphous-crystalline transition [11,12], and perovskite oxides ($A_{1-X}B_XMo_3$) [13,14] and vanadium dioxide (VO_2) [15,16] with metal-insulator transition. The phase changing temperature of $Ge_2Sb_2Te_5$ is too high (~931 K) [11,12], and the temperature range of perovskite oxides during the phase transition is too large (~200 K) [13], both of which face huge obstacles in the practical application of spacecraft thermal control. The requirement for transition temperature of the thermochromic film for human spacecraft is typically dictated by the needs of the avionics downstream of the radiator outlet. Avionics and similar electronic components can only work around room temperature (268~318 K) [1,2]. Therefore, VO_2 is a more favorable phase change material for spacecraft applications due to its dramatic change of optical properties at phase change point (~340 K) near room temperature [16]. Meanwhile, the transition temperature of VO_2 can be decreased by doping VO_2 with tungsten [16,17].

In addition to the phase transition temperature, the radiative characteristic of the thermochromic film also plays a vital role in the application of spacecraft thermal control. Firstly, the infrared emittance ε of the thermochromic film at high temperature is expected to be as large as possible in order to efficiently dissipate the internal thermal loads into the space, which is the basis of the spacecraft thermal control [2]. Generally, the infrared emittance of the traditional thermal control coatings is larger than 0.80, such as an optical solar reflector (ε>0.80), a white paint (ε>0.87) and a black paint (ε>0.88) [2]. Meanwhile, the solar absorptance a_{solar} of the thermal control coatings needs to be small enough ($a_{solar} < 0.20$) especially when the radiating surface is in the sunward side of the spacecraft, since the solar radiance is the main source of the external heat flux. When the radiating surface is in the nightside, low solar absorptance of the coatings is not a necessary requirement. However, there are very few missions where the radiating surface can be completely kept out of sun. For thermochromic film with large solar absorption, some optimal scheme is needed to reduce the solar absorptance, such as adding layers with high solar reflectivity and infrared transmittance. Moreover, the emittance tunability $\Delta\varepsilon$ of the thermochromic film needs to be large enough to deal with the violent alternation of thermal environment. However, both the infrared emittance at high temperature and emittance tunability of the thermochromic film made solely of phase change materials are far from satisfying the needs of spacecraft. In order to enlarge the emittance tunability of the thermochromic film, thermochromic materials are usually combined with other functional materials to form composite micro/nano structures, including multilayer films [18–23], micro/nano particle composite films [24,25] and photonic crystal films [26–28].

The VO_2-based Fabry-Perot (FP) multilayer films attract tremendous attention due to its simple structure, suitable phase change temperature and enhanced emittance tunability by FP resonance. Hendaoui et al. [18] synthesized a VO_2 based smart film which is made of 850 nm thick SiO_2 layer sandwiched between a thin VO_2 front layer with a thickness of 30 nm and a highly reflecting back Au layer. The infrared emittance of the device was found to be 0.22 and 0.71 at 25 °C and 100 °C, respectively. Taylor et al. [19] numerically elucidated the physical mechanisms of the

Optics EXPRESS

absorption enhancements of the VO_2-based FP multilayer films by examining the total phase shift in the multilayer structure and the phonon modes of VO_2. Kim et al. [20] synthesized a multilayer structure ($Si/VO_2/BaF_2/Au$) for spacecraft thermal control. The emittance tunability of the multilayer structure can reach about 0.49 with an infrared emittance of 0.64 at high temperature. Shrewsbury et al. [21] proposed a device based on a multilayer stack of VO_2, ZnSe and gold. The emittance tunability of the multilayer stack is 0.69 with a high temperature emittance equal to 0.77. However, the FP resonance is limited in a narrow band, which restricts the further increase of the infrared emittance and emittance tunability of the VO_2-based FP multilayer film. Table 1 illustrates the performances of existing typical thermochromic thermal control films. As observed in Table 1, the infrared emittance of most existing thermochromic films under metallic state is less than 0.77, which is far from that of traditional thermal control coatings. Moreover, there is still much room for improvement in the aspect of large-range emittance tuning.

Table 1. The performances of existing typical thermochromic thermal control films.

Film types	Film structure and materials	ε[a]	$\Delta\varepsilon$[c]	Spectral range	EXP/SIM[d]
Traditional thermal control coatings	*optical solar reflector*	*0.80*	–	Entire infrared	EXP
	white paint	*0.87*	–	Entire infrared	EXP
	black paint	*0.88*	–	Entire infrared	EXP
Particle composite film	VO_2 particle composite film [5]	0.65[b]	0.45	Entire infrared	EXP
	VO_2 nanopowder pellets [24]	0.36	−0.46	8~14 μm	EXP
	CaF_2@VO_2 particles composite film [25]	0.83	0.36	4~14 μm	EXP
Photonic crystal film	patterned VO_2 meta-surface [29]	0.75	0.48	2.5~25 μm	EXP
	trapezoidal VO_2-Ge multilayer [30]	0.87	0.67	8~13 μm	SIM
Multilayer film	$VO_2/SiO_2/Au$ multilater [16,18]	0.71	0.49	2.5~25 μm	EXP
	$Si/VO_2/BaF_2/Au$ multilayer [20]	0.64	0.49	2~25 μm	EXP
	$VO_2/ZnSe/VO_2/ZnSe/Au$ multilayer [21]	0.77	0.69	2~30 μm	SIM
	$VO_2/MgF_2/W + Ge/MgF_2$ multilayer [22]	0.636	0.582	8~13 μm	SIM
	Mo/VO_2/nanocrystal multilayer [23]	0.867	0.568	8~13 μm	SIM
This work	superposed FP film (sol-gel)	0.95	0.78	2.5~30 μm	SIM
	superposed FP film (magnetron sputtering)	0.91	0.70	2.5~30 μm	SIM

[a]In the third column, the infrared emittance ε of the thermochromic film under metallic state are listed except Ref. [5].
[b]In Ref. [5], the maximum emissivity of the film is obtained for VO_2 under semi-metallic state.
[c]In the fourth column, the emittance tunability $\Delta\varepsilon$ is equal to the infrared emittance at high temperature minus that at low temperature as described in detail in Section 2.
[d]These data in Table 1 are obtained either by experiment (EXP) or by simulation (SIM) as listed in the last column.

Herein, a VO_2-based superposed FP multilayer film is proposed for spacecraft thermal control, which supports three FP resonances at different peak wavelengths. The superposed FP film is constructed by encapsulating three thin VO_2 layers in four lossless BaF_2 spacers on an Al substrate. The effect of each layer thickness on the radiation characteristics of the superposed FP film is studied, and the thickness of each layer is optimized in terms of the infrared emittance and emittance tunability. For the typical growth techniques of the VO_2 layers considered here, the emittance tunability of the superposed FP film can exceed 0.70 with total normal emittance larger than 0.91 at high temperature. The largest total normal emittance of the superposed film can reach 0.95 with emittance tunability of 0.78. In addition, the infrared emittance and emittance tunability of the superposed FP film remain large in a very wide incident angle range.

Optics EXPRESS

2. Design of multilayer film

Figure 1(a) shows the sketch of the FP multilayer structure. As shown in Fig. 1(a), a dielectric spacer is placed between a thin top mirror and a reflecting substrate to form a FP resonance which dramatically enhances the absorption of the film but is limited in a narrow band. Figure 2 illustrates the refractive index n and absorption index κ of the VO_2 film as a function of wavelength λ under dielectric state and metallic state [15,31,32]. As can be seen in Fig. 2, VO_2 switches between dielectric state (low loss, semitransparent) and metallic state (lossy, more reflective) in the infrared spectral range. For the VO_2 layer under dielectric state, the multilayer structure is highly reflective due to the reflecting substrate, since the insulating VO_2 layer and the spacer are highly transparent in the mid infrared spectral range. However, when VO_2 is under metallic state, the VO_2 layer serves as a top mirror to form a FP resonant material, generating an enhanced absorption in the mid-infrared spectral range.

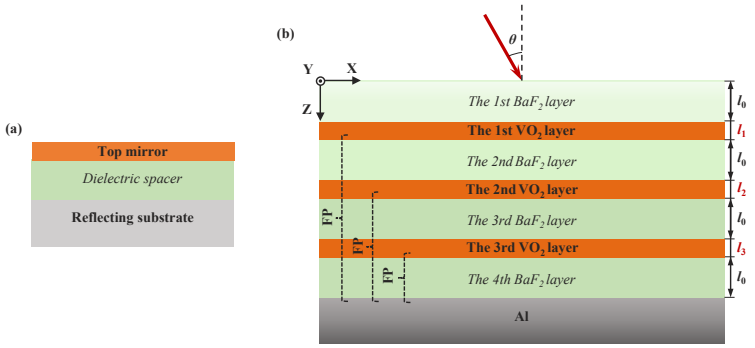

Fig. 1. (a) The sketch of the FP multilayer structure; (b) The sketch of the VO_2-based superposed FP multilayer film. Three VO_2 layers with different thicknesses are encapsulated in four BaF_2 layers with the same thickness on an Al substrate to construct three FP resonances at different peak wavelengths.

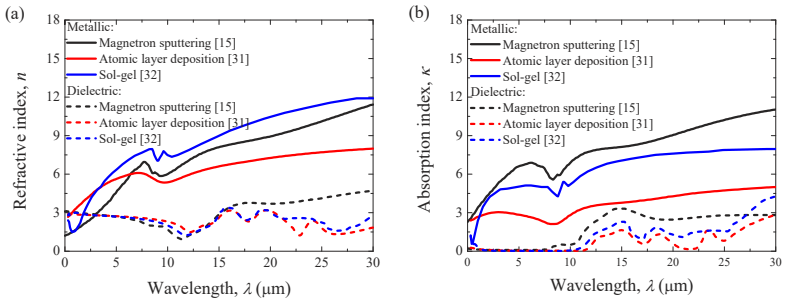

Fig. 2. (a) The refractive index n and (b) absorption index κ of the VO_2 film as a function of wavelength λ under dielectric state and metallic state. The VO_2 film samples used in the complex refractive index measurements were synthesized by using magnetron sputtering [15], atomic layer deposition [31] and sol-gel [32], respectively.

In order to enlarge the infrared emittance (in the whole mid-infrared spectral range) and emittance tunability, the VO_2-based superposed FP multilayer film is designed to form multiple FP resonances. Figure 1(b) shows the sketch of the VO_2-based superposed FP multilayer film. As can be seen in Fig. 1(b), the superposed FP film is composed of three VO_2 layers, four BaF_2 layers and an Al substrate. The Al substrate is chosen as the reflecting substrate of the FP resonant

Optics EXPRESS

material, and the complex refractive index of Al published in Ref. [34] is used in our calculation. For the dielectric spacer, a broadband transparent material is preferred for the enhancement of the emittance tunability. BaF_2 is chosen as the dielectric spacer which has almost no absorption in the spectral range from 2.5 to 20 µm. Figure 3 shows the refractive index n and absorption index κ of BaF_2 film as a function of wavelength λ [33]. In addition, the outermost BaF_2 layer is designed to serve as anti-reflective layer to further increase the absorption of the superposed FP film.

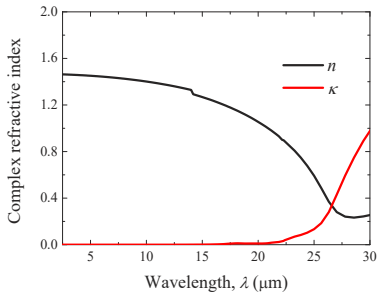

Fig. 3. The refractive index n and absorption index κ of the BaF_2 [33] film as a function of wavelength λ.

In order to construct a multiple FP resonances VO_2-BaF_2-Al stack, three VO_2 layers are encapsulated in four BaF_2 layers, as shown in Fig. 1(b). In general, the amplitude and the width of the FP resonance can be tuned by the top mirror thickness, and the resonance wavelength is dependent on the spacer thickness [19,20,35]. The required spacer thickness l to achieve a FP resonance at the target wavelength λ can be predicted by [35]:

$$l = \frac{m\lambda}{4n} \tag{1}$$

where m is an odd integer, and n is the refractive index of the spacer. In this work, the thicknesses of each VO_2 layers are different, but the thicknesses of the four BaF_2 layers are designed to be uniform, thus the peak wavelengths of the three FP resonances can be almost uniformly spaced. For spacecraft thermal control, the spectral emittance is expected to be close to unity in the mid-infrared spectral range. In order to obtain a large infrared emittance, the three FP resonances should be uniformly spaced in the spectral range where the spectral exitance of a blackbody is strong. The spectral exitance of a blackbody at a temperature of 300 K peaks at the wavelength of about 9 µm and exhibits a relatively large exitance in the spectral range 5~25 µm. Therefore, according to formula (1), the thickness of the BaF_2 layer should vary around 1.5 µm with $m = 1$, corresponding to the resonance wavelengths of about 9, 15 and 20 µm. It should be noted that the target wavelengths of the FP resonances are just estimated values so that the thickness of the BaF_2 layer can be limited in a proper range to avoid brute-force calculations. In this work, VO_2 layers with thicknesses in the range of 5~50 nm (interval is 5 nm), and BaF_2 layers with thicknesses in the range of 0.5~2.0 µm (interval is 0.1 µm) are modeled to optimize the infrared emittance and emittance tunability of the superposed FP film.

Spectral directional emittance can be obtained by calculating the spectral directional hemispherical reflectance of a film. According to Kirchhoff's law, the spectral directional emittance $\varepsilon_{\lambda,\theta}$ and spectral directional absorptance $a_{\lambda,\theta}$ of a body are equal at any specified temperature and wavelength at thermal equilibrium conditions. Therefore, the spectral directional emittance of an opaque material can be expressed by:

$$\varepsilon_{\lambda,\theta} = 1 - R_{\lambda,\theta} \tag{2}$$

Optics EXPRESS

where $R_{\lambda,\theta}$ is the spectral directional hemispherical reflectance with incident angle θ (including the specular and the diffuse components of the reflectance). The spectral directional hemispherical reflectance of the multilayer film is calculated by the Rigorous Coupled Wave Analysis (RCWA) method [36,37]. The total directional emittance ε_θ can be obtained by integrating the spectral directional emittance in the infrared spectral range:

$$\varepsilon_\theta = \frac{\int_{2.5\mu m}^{30\mu m} \varepsilon_{\lambda,\theta} I_B(\lambda, T) d\lambda}{\int_{2.5\mu m}^{30\mu m} I_B(\lambda, T) d\lambda} \tag{3}$$

where $I_B(\lambda, T)$ is the spectral exitance of a blackbody at temperature T given by Planck's function. The spectral range from 2.5 to 30 μm is considered in this work, corresponding to main emission band of a blackbody at a temperature of 300 K. The emittance tunability $\Delta\varepsilon_\theta$ is defined as the difference of total directional emittance between metallic and dielectric state of the VO_2 layers:

$$\Delta\varepsilon_\theta = \varepsilon_{m,\theta} - \varepsilon_{d,\theta} \tag{4}$$

where $\varepsilon_{m,\theta}$ is the total directional emittance of the thermochromic film under metallic state, and $\varepsilon_{d,\theta}$ is the total directional emittance of the thermochromic film under dielectric state.

3. Results and analysis

In this section, the complex refractive index of a VO_2 film synthesized by magnetron sputtering [15] (see Fig. 2) was used to comprehensively show the radiative properties of the superposed FP film and interpret the physical mechanism. Figure 4(a) shows the total normal emittance ε_{normal} and emittance tunability $\Delta\varepsilon_{normal}$ of the VO_2-based superposed FP multilayer film as a function of the thickness l_1 of the first VO_2 layer with $l_2 = 10$ nm, $l_3 = 30$ nm and $l_0 = 1.5$ μm. As shown in Fig. 4(a), the total normal emittance of the superposed FP film for VO_2 layers under metallic state decreases monotonously with increasing thickness of the first VO_2 layer, while for VO_2 layers under dielectric state it increases monotonously, leading to a decreased emittance tunability. Thus, the smaller the thickness l_1 of the first VO_2 layer is, the larger the total normal emittance and emittance tunability is. Figure 4(b) presents the total normal emittance ε_{normal} and emittance tunability $\Delta\varepsilon_{normal}$ of the VO_2-based superposed FP multilayer film as a function of the thickness l_2 of the second VO_2 layer with $l_1 = 10$ nm, $l_3 = 30$ nm and $l_0 = 1.5$ μm. As shown in Fig. 4(b), with increasing thickness of the second VO_2 layer, the total normal emittance of the superposed FP film for VO_2 layers under metallic state decreases monotonously, while for VO_2 layers under dielectric state it increases monotonously, leading to a decreased emittance tunability. Therefore, similar to the first VO_2 layer, a smaller thickness l_2 of the second VO_2 layer is preferred to obtain a larger total normal emittance and emittance tunability of the superposed FP film.

Figure 4(c) shows the total normal emittance ε_{normal} and emittance tunability $\Delta\varepsilon_{normal}$ of the VO_2-based superposed FP multilayer film as a function of the thickness l_3 of the third VO_2 layer with $l_1 = l_2 = 10$ nm and $l_0 = 1.5$ μm. As observed in Fig. 4(c), with increasing thickness of the third VO_2 layer, the total normal emittance of the superposed FP film for VO_2 layers under metallic state firstly increases when $l_3 < 30$ nm, and then decreases slightly when $l_3 > 30$ nm. While for VO_2 layers under dielectric state it increases monotonously, leading to a decreased emittance tunability. Therefore, it seems that the superposed FP film with l_3 equal to 30 nm tends to obtain a large total normal emittance and emittance tunability. Overall, the effect of the thickness of the outer VO_2 layer on the total normal emittance and emittance tunability of the superposed FP film is significant. On the contrary, the total normal emittance and emittance tunability of the superposed FP film are almost independent on the thickness of the inner VO_2 layer. It can be explained by the fact that the outer VO_2 layer interacts with the primary incident wave,

Optics EXPRESS

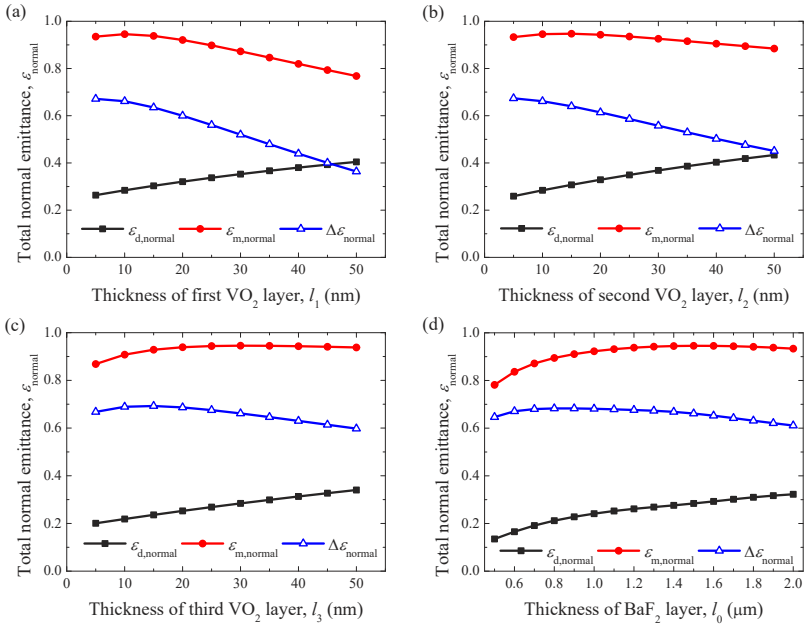

Fig. 4. (a) The total normal emittance ε_{normal} and emittance tunability $\Delta\varepsilon_{normal}$ of the VO_2-based superposed FP multilayer film as a function of the thickness l_1 of the first VO_2 layer with $l_2 = 10$ nm, $l_3 = 30$ nm and $l_0 = 1.5$ μm; (b) The total normal emittance ε_{normal} and emittance tunability $\Delta\varepsilon_{normal}$ of the VO_2-based superposed FP multilayer film as a function of the thickness l_2 of the second VO_2 layer with $l_1 = 10$ nm, $l_3 = 30$ nm and $l_0 = 1.5$ μm; (c) The total normal emittance ε_{normal} and emittance tunability $\Delta\varepsilon_{normal}$ of the VO_2-based superposed FP multilayer film as a function of the thickness l_3 of the third VO_2 layer with $l_1 = l_2 = 10$ nm and $l_0 = 1.5$ μm; (d) The total normal emittance ε_{normal} and emittance tunability $\Delta\varepsilon_{normal}$ of the VO_2-based superposed FP multilayer film as a function of the thickness l_0 of the BaF_2 layer with $l_1 = l_2 = 10$ nm and $l_3 = 30$ nm. The total normal emittance is obtained by integrating the spectral normal emittance in the infrared spectral range from 2.5 to 30 μm.

i.e., the strongest intensity of incident wave for the FP resonance, leading to a more dramatical interference between the film and the electromagnetic wave.

Figure 4(d) shows the total normal emittance ε_{normal} and emittance tunability $\Delta\varepsilon_{normal}$ of the VO_2-based superposed FP multilayer film as a function of the thickness l_0 of the BaF_2 layer with $l_1 = l_2 = 10$ nm and $l_3 = 30$ nm. As shown in Fig. 4(d), with increasing thickness of the BaF_2 layer, the total normal emittance of the superposed FP film for VO_2 layers under both states increases monotonously. For VO_2 layers under metallic state, the thickness of the BaF_2 layer primarily influences the resonant wavelength of the FP resonance. Therefore, the total normal emittance tends to increase until perfect thickness of the BaF_2 layer is achieved. For VO_2 layers under dielectric state, on the other hand, the increased thickness of the BaF_2 layer leads to an increased emittance in the spectral range from 20 to 30 μm, thus the total normal emittance of the superposed FP film increases. Moreover, the emittance tunability decreases slightly with increasing thickness of the BaF_2 layer. In summary, for VO_2-based superposed FP multilayer film with $l_0 = 1.0$ μm, $l_1 = l_2 = 10$ nm, and $l_3 = 15$ nm, the emittance tunability can exceed 0.70 with total normal emittance larger than 0.91, simultaneously. For VO_2-based superposed FP multilayer film with $l_0 = 1.5$ μm, $l_1 = l_2 = 10$ nm, and $l_3 = 30$ nm, a maximum total normal emittance ($\varepsilon_{normal} = 0.95$) is obtained with emittance tunability of 0.67.

Optics EXPRESS

In order to better understand the enhancement mechanism, Fig. 5 illustrates the spectral normal emittance $\varepsilon_{\lambda,\text{normal}}$ of the VO_2-based superposed FP multilayer film with a maximum total normal emittance at high temperature in the spectral range from 2.5 to 30 µm with normal plane wave incidence. The thickness of each layer of the superposed FP film in Fig. 5 is $l_0 = 1.5$ µm, $l_1 = l_2 = 10$ nm, and $l_3 = 30$ nm, respectively. As can be seen in Fig. 5, for VO_2 layers under metallic state, the spectral normal emittance of the superposed FP film is larger than 0.95 in the spectral range from 5 to 22 µm (i.e., the major emission band of a blackbody at a temperature of 300 K), resulting in a total normal emittance of 0.95. In the spectral range from 20 to 30 µm, the spectral normal emittance decreases monotonously with increasing wavelength due to the large complex refractive index of VO_2 layers. For VO_2 layers under dielectric state, the superposed FP film only exhibits significant spectral normal emittance when the wavelength is larger than 15 µm, while in the spectral range from 2.5 to 15 µm there is almost no absorption/emission, resulting in a total normal emittance of 0.28.

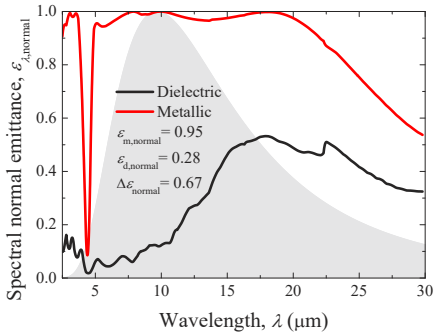

Fig. 5. The spectral normal emittance $\varepsilon_{\lambda,\text{normal}}$ of the VO_2-based superposed FP multilayer film for VO_2 layers under metallic and dielectric state in the spectral range from 2.5 to 30 µm, the thickness of each layer is $l_0 = 1.5$ µm, $l_1 = l_2 = 10$ nm, and $l_3 = 30$ nm, respectively. The shaded area is the spectral exitance $I_B(\lambda, T)$ of a blackbody at a temperature of 300 K given by Planck's function.

The large emittance of the superposed FP film is attributed to the absorption of the three metallic VO_2 layers due to the superposed FP resonances at specific wavelengths. Figure 6 presents the spectral normal emittance ε_λ of each layer of the superposed FP film for VO_2 layers under (a, c) metallic and (b, d) dielectric state in the spectral range from 2.5 to 30 µm with normal plane wave incidence. The thickness of each layer of the superposed FP film in Fig. 5 is $l_0 = 1.5$ µm, $l_1 = l_2 = 10$ nm, and $l_3 = 30$ nm, respectively. As shown in Fig. 6(a), due to the FP resonance, the spectral normal emittance of the first, second and third VO_2 layer peaks at wavelengths of about 20, 15 and 9 µm, respectively, corresponding to the three FP resonances VO_2-BaF_2-Al stacks in Fig. 1(b) with dielectric spacer thicknesses of about 4.5, 3.0 and 1.5 µm. The intensity of each FP resonance is weakened due to the decreased intensity of the reflected wave by the other two thin VO_2 layers, resulting in lower absorption of each VO_2 layer. However, by combining the three FP resonances, a nearly perfect absorption/emission (i.e., a spectral normal emittance close to 1) of the total multilayer film is obtained in the spectral range from 5 to 20 µm. For VO_2 layers under dielectric state, the superposed FP film becomes more reflective due to the bottom reflecting Al substrate and highly transparent VO_2 and BaF_2 layers. The total normal emittance of the superposed FP film is primarily attributed to the absorption of the VO_2 layers in the spectral range from 10 to 20 µm and the BaF_2 layers in the spectral range from 20 to 30 µm as shown in Fig. 6(b) and 6(d).

Figure 7 shows the normalized electric field $|E/E_0|$ (E_0 is the incident electric field) of the VO_2-based superposed FP multilayer film for VO_2 layers under (a-d) metallic state and (e-h)

Optics EXPRESS

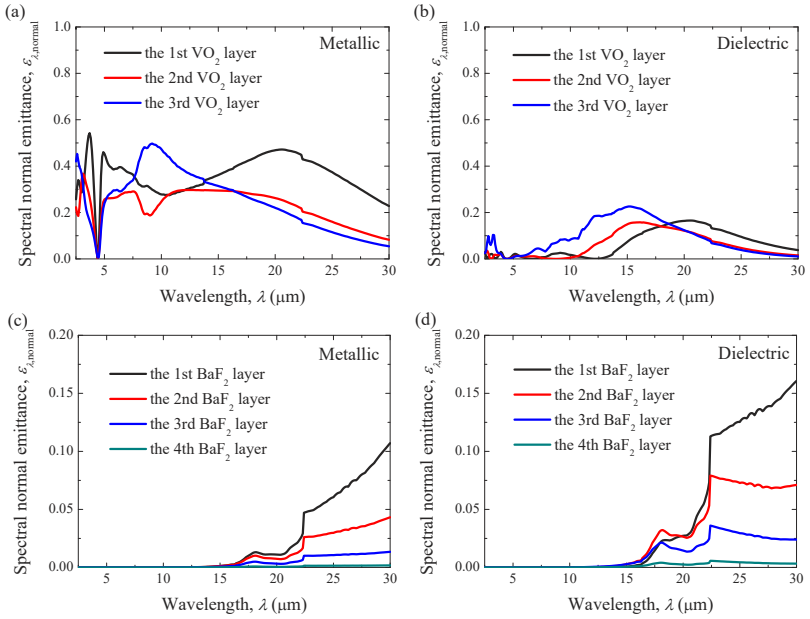

Fig. 6. The spectral normal emittance $\varepsilon_{\lambda,\text{normal}}$ of each layer of the VO_2-based superposed FP multilayer film for VO_2 layers under (a, c) metallic and (b, d) dielectric state in the spectral range from 2.5 to 30 μm with normal plane wave incidence. The thickness of each layer is $l_0 = 1.5$ μm, $l_1 = l_2 = 10$ nm, and $l_3 = 30$ nm, respectively.

dielectric state at the wavelengths of 4.4, 9, 15 and 20 μm, respectively. The thickness of each layer of the superposed FP film in Fig. 7 is $l_0 = 1.5$ μm, $l_1 = l_2 = 10$ nm, and $l_3 = 30$ nm, respectively. As shown in Fig. 7(a) and 7(e), the incident and reflected waves dramatically interfere with each other at the wavelength of 4.4 μm for VO_2 layers under both states, form an obvious enhanced and restricted electric field compared to the incident electric field. The VO_2 layers are just located at the restricted regions with electric field of almost zero, leading to an extremely small emission of the total multiple film as shown in Fig. 5. For the superposed FP film with VO_2 layers under metallic state at the resonance wavelengths, as shown in Figs. 7(b-d), the electric field tends to decrease monotonously along Z axis direction (i.e., the incident direction). Almost no interference between the incident and reflected waves can be observed due to the perfect absorption caused by the superposed FP resonances in the spectral range from 5 to 22 μm. While for VO_2 layers under dielectric state, the whole VO_2 and BaF_2 layers become semi-transparent, strong interferences between the incident and reflected waves are observed in Figs. 7(f-h).

Figure 8 shows the spectral and incident angle dependent emittance contours of the VO_2-based superposed FP multilayer film for VO_2 layers under metallic state with (a) Transverse Electric (TE) wave and (b) Transverse Magnetic (TM) wave, and dielectric state with (c) TE wave and (d) TM wave. The thickness of each layer of the superposed FP film in Fig. 8 is $l_0 = 1.5$ μm, $l_1 = l_2 = 10$ nm, and $l_3 = 30$ nm, respectively. As can be seen in Figs. 8(a-b), for the superposed FP film with VO_2 layers under metallic state, the spectral directional emittance varies little with increasing incident angle in the spectral range from 5 to 20 μm when the incident angle is less than 45° for both TE and TM waves, while in the spectral range from 20 to 30 μm it is more sensitive to the incident angle. For incident angles larger than 45°, the spectral directional emittance tends to decrease obviously with increasing incident angle. For the superposed FP film with VO_2 layers under dielectric state, as shown in Figs. 8(c-d), the spectral directional emittance seems to be independent on the incident angle when the incident angle is less than 60° and keeps

Optics EXPRESS

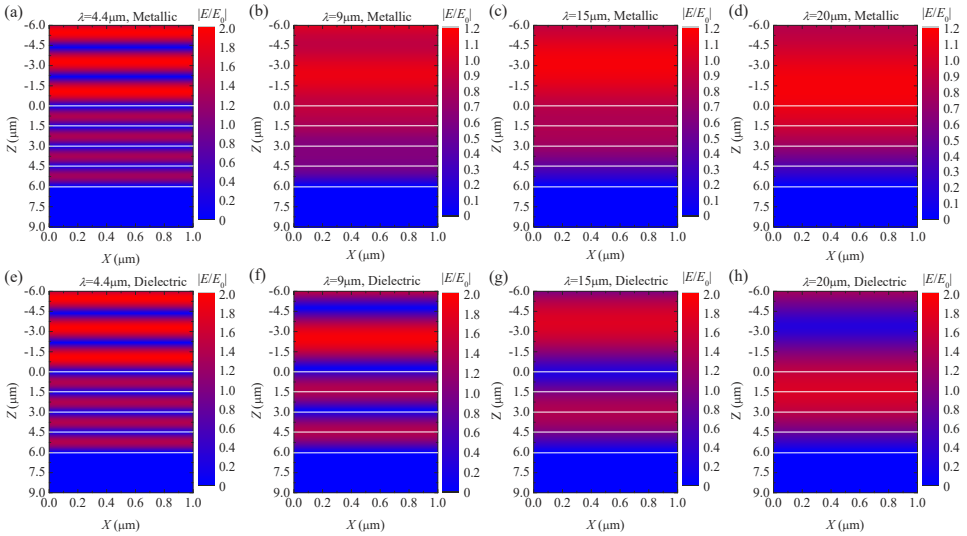

Fig. 7. The normalized electric field $|E/E_0|$ of the VO_2-based superposed FP multilayer film for VO_2 layers under (a-d) metallic state and (e-h) dielectric state at the wavelengths of 4.4, 9, 15 and 20 μm, respectively. The thickness of each layer is $l_0 = 1.5$ μm, $l_1 = l_2 = 10$ nm, and $l_3 = 30$ nm, respectively. E_0 is the incident electric field, and the incident direction is normal to the layers. The white lines represent the boundaries of each layer. Only the BaF_2 layers can be clearly seen in the figures, due to the VO_2 layers too thin to be represented.

at a relatively small value (<0.5) in the spectral range from 2.5 to 30 μm. Discontinuities in the spectral directional emittance of the superposed FP film are observed at a wavelength of about 22.5 μm in Fig. 8. It is due to the sudden increase of the spectral directional emittance of the BaF_2 layers as can be seen in Figs. 6(c-d). Spectral directional emittance with values close to unity can be observed for VO_2 layers under dielectric state with both TE and TM waves, but it is still confined in a narrow spectral range and incident angle range. The areas of high spectral directional emittance for VO_2 layers under dielectric state can be explained as below. The reflectance of the dielectric VO_2-BaF_2 interface increases with the incident angle. With such increased interfacial reflectance, it tends to form a FP resonance in the spectral range from 15 to 30 μm where the absorption index is large enough as shown in Fig. 2(b). Similar phenomenon and explanations can be seen in Refs. [19,38].

Figure 9 shows the total directional emittance ε_θ of the VO_2-based superposed FP multilayer film for VO_2 layers under metallic state and dielectric state with TE wave and TM wave as a function of the incident angle. The thickness of each layer of the superposed FP film in Fig. 9 is $l_0 = 1.5$ μm, $l_1 = l_2 = 10$ nm, and $l_3 = 30$ nm, respectively. As shown in Fig. 9, for VO_2 layers under metallic state, the total directional emittance of the superposed FP film with TE and TM waves remains larger than 0.9 for incident angles up to 45° and 60°, respectively, indicating that the total directional emittance with TE wave is more sensitive to incident angle than that of TM wave. For VO_2 layers under dielectric state, the total directional emittance of the superposed FP film seems to be independent of the incident angle for both TE and TM waves for incident angles up to 60°. Generally, for both TE and TM waves, a large total directional emittance at high temperature and high emittance tunability of the superposed FP film is obtained even with incident angles up to 60°. These results show that the total directional emittance and emittance tunability of the superposed FP film possesses excellent insensitivity against both the incident angle and wave polarization.

Optics EXPRESS

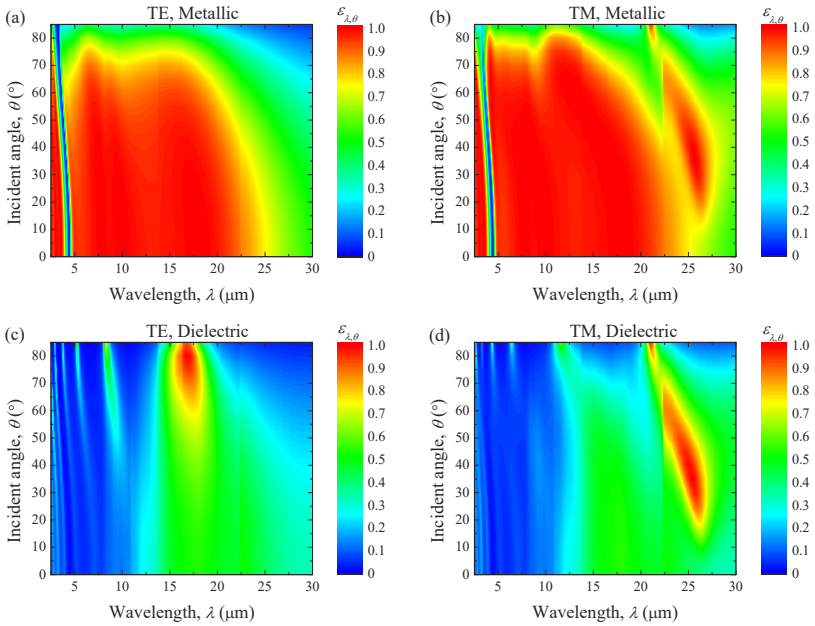

Fig. 8. The spectral and incident angle dependent emittance contours of the VO_2-based superposed FP multilayer film for VO_2 layers under metallic state with (a) TE wave and (b) TM wave, and dielectric state with (c) TE wave and (d) TM wave. The thickness of each layer of the multilayer film is $l_0 = 1.5\,\mu m$, $l_1 = l_2 = 10\,nm$, and $l_3 = 30\,nm$, respectively.

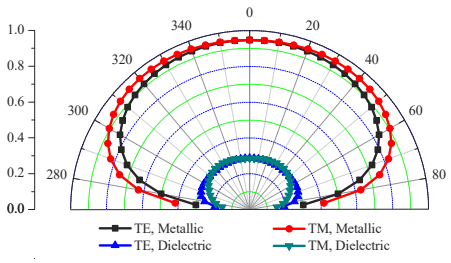

Fig. 9. The total directional emittance ε_θ of the VO_2-based superposed FP multilayer film for VO_2 layers under metallic and dielectric state with TE wave and TM wave as a function of the incident angle. The thickness of each layer is $l_0 = 1.5\,\mu m$, $l_1 = l_2 = 10\,nm$, and $l_3 = 30\,nm$, respectively.

Optics EXPRESS

Last but not least, the complex refractive index of VO_2 layers in the visible and infrared spectral range obtained by experimental measurements are different throughout the literature [15,20,31,32], as shown in Fig. 2. It can be explained by the fact that the growth technique influences the optical properties due to the quality of the thin crystalline films [31,32]. Despite the variation of the complex refractive index of VO_2, the physical mechanism of the superposed FP film is general. Therefore, the limited difference in the complex refractive index of the VO_2 layers will not affect the acquisition of excellent performance of the superposed FP film. Table 2 illustrates the performances and the optimal film structure parameters of the superposed FP film for VO_2 layers synthesized by typical growth techniques, including magnetron sputtering, atomic layer deposition and sol-gel. As shown in Table 2, for VO_2 layers synthesized by different growth techniques, the excellent performances of the superposed FP film can be obtained by adjusting the layer thickness. Generally, the emittance tunability of the superposed FP film can exceed 0.70 with total normal emittance larger than 0.91 at high temperature. For VO_2 layers synthesized by sol-gel method, the largest total normal emittance of the superposed FP film can reach 0.95 with emittance tunability of 0.78.

Table 2. The performances and the optimal film structure parameters of the superposed FP film for VO_2 layers synthesized by typical growth techniques.

Growth technique	Film structure parameters				Total normal emittance $\varepsilon_{m,normal}$ (metallic)	Emittance tunability $\Delta\varepsilon$
	l_0 (μm)	l_1 (nm)	l_2 (nm)	l_3 (nm)		
Magnetron sputtering [15]	1.0	10	10	15	0.91	0.70
Atomic layer deposition [31]	1.5	20	30	50	0.94	0.73
Sol-gel [32]	1.5	10	10	30	0.95	0.78

It should be noted that lowering the VO_2 phase transition temperature is also essential for making VO_2-based thermochromic film viable for spacecraft applications. Generally, spacecraft applications will be targeting a transition temperature between room temperature and ~10 °C. The transition temperature of VO_2 can be decreased by doping VO_2 with tungsten [16,17]. It seems that doping W would not significantly affect the complex refractive index of VO_2 [16,17,39], and thus would not affect much the excellent radiation characteristic of the superposed FP film.

4. Conclusion

In this work, a VO_2-based superposed FP multilayer film with simple structure, nearly perfect infrared emission (i.e., an infrared emittance close to 1) and large emittance tunability was proposed for spacecraft thermal control. The superposed FP film is constructed by encapsulating three thin VO_2 layers in four lossless BaF_2 spacers on the Al substrate to form multiple FP resonances. The effect of the thickness of each layer on the infrared emittance and emittance tunability of the superposed FP film was studied to achieve a maximum infrared emittance and emittance tunability. Generally, for the typical growth techniques of the VO_2 layers considered here, the emittance tunability of the superposed FP film can exceed 0.70 with total normal emittance larger than 0.91 at high temperature, simultaneously. For VO_2 layers synthesized by sol-gel method, the largest total normal emittance of the superposed FP film can reach 0.95 with emittance tunability of 0.78. The spectral normal emittance of the superposed FP film is near unity for VO_2 layers under metallic state in the spectral range from 5 to 20 μm, due to the three superposed FP resonances. While for VO_2 layers under dielectric state, the superposed FP film becomes more reflective especially in the spectral range from 2.5 to 11.5 μm with a spectral normal emittance less than 0.2. In addition, the infrared emittance and emittance tunability performances remain large for an incident angle up to 60°. The structure proposed in this work

Optics EXPRESS

outperforms the existing thermochromic films in literature, which could accelerate the application of thermochromic films in the field of spacecraft thermal control.

Funding. National Natural Science Foundation of China (52106103, 52076123); Natural Science Foundation of Shandong Province (ZR2020QE194).

Disclosures. The authors declare that there are no conflicts of interest related to this paper

Data availability. Data underlying the results presented in this paper are not publicly available but may be obtained from the authors upon reasonable request.

References

1. P. Fortescue, G. Swinerd, and J. Stark, *Spacecraft systems engineering* (John Wiley & Sons, 2011).
2. J. Miao, Q. Zhong, Q. Zhao, and X. Zhao, *Spacecraft Thermal Control Technologies* (Springer, 2021).
3. M Grob L and S Theodore D, "Parametric study of variable emissivity radiator surfaces," **504**, 809–814 (2000).
4. National Academies of Sciences, *Engineering, and Medicine, NASA space technology roadmaps and priorities revisited* (National Academies Press, 2016).
5. R. V. Kruzelecky, E. Haddad, B. Wong, and W. R. Jamroz, "Variable emittance thermochromic material and satellite system," US7761053B2 (2010).
6. F. Lang, H. Wang, S. Zhang, J. Liu, and H. Yan, "Review on variable emissivity materials and devices based on smart chromism," Int. J. Thermophys. **39**(1), 6–20 (2018).
7. E Franke, H Neumann, M Schubert, L Trimble C, Y Li, and A Woollam J, "Low-orbit-environment protective coating for all-solid-state electrochromic surface heat radiation control devices," Surf. Coat. Technol. 151-152, 285-288 (2002).
8. H. Demiryont and D. Moorehead, "Electrochromic emissivity modulator for spacecraft thermal management," Sol. Energy Mater. Sol. Cells **93**(12), 2075–2078 (2009).
9. R. Osiander, J. Champion, M. Darrin, J. Allen, and T. Swanson, "Micro-machined shutter arrays for thermal control radiators on ST5," *40th AIAA Aerospace Sciences Meeting & Exhibit*, 0359 (2002).
10. D. Xu, J. Zhao, and L. Liu, "Near-field radiation assisted smart skin for spacecraft thermal control," Int. J. Therm. Sci. **165**, 106934 (2021).
11. B. Gholipour, J. Zhang, K. F. MacDonald, D. W. Hewak, and N. I. Zheludev, "An all-optical, non-volatile, bidirectional, phase-change meta-switch," Adv. Mater. **25**, 3050–3054 (2013).
12. K. Du, Q. Li, Y. Lyu, J. Ding, Y. Lu, Z. Cheng, and M. Qiu, "Control over emissivity of zero-static-power thermal emitters based on phase-changing material GST," Light: Sci. Appl. **6**(1), e16194 (2017).
13. Y. Shimakawa, T. Yoshitake, Machida Kubo, K. Shinagawa, and A. Okamoto, "A variable-emittance radiator based on a metal–insulator transition of (La,Sr)MnO_3 thin films," Appl. Phys. Lett. **80**(25), 4864–4866 (2002).
14. S. Tachikawa, A. Ohnishi, Y. Shimakawa, A. Ochi, A. Okamoto, and Y. Nakamura, "Development of a Variable Emittance Radiator Based on a Perovskite Manganese Oxide," J. Thermophys Heat Transfer **17**(2), 264–268 (2003).
15. M. Benkahoul, M. Chaker, J. Margot, E. Haddad, R. Kruzelecky, B. Wong, W. Jamroz, and P. Poinas, "Thermochromic VO_2 film deposited on Al with tunable thermal emissivity for space applications," Solar Energy Materials & Solar Cells **95**(12), 3504–3508 (2011).
16. A. Hendaoui, N. émond, S. Dorval, M. Chaker, and E. Haddad, "VO_2-based smart coatings with improved emittance-switching properties for an energy-efficient near room-temperature thermal control of spacecrafts," Solar Energy Materials & Solar Cells **117**, 494–498 (2013).
17. M. Tazawa, P. Jin, and S. Tanemura, "Optical constants of $V_{1-x}W_xO_2$ films," Appl. Opt. **37**(10), 1858–1861 (1998).
18. A. Hendaoui, N. Emond, M. Chaker, and E. Haddad, "Highly tunable-emittance radiator based on semiconductor-metal transition of VO_2 thin films," Appl. Phys. Lett. **102**(6), 525 (2013).
19. S. Taylor, Y. Yang, and L. Wang, "Vanadium dioxide based Fabry-Perot emitter for dynamic radiative cooling applications," J. Quant. Spectrosc. Radiat. Transfer **197**, 76–83 (2017).
20. H. Kim, K. Cheung, R. Auyeung, D. E. Wilson, and N. A. Charipar, "VO_2-based switchable radiator for spacecraft thermal control," Sci. Rep. **9**(1), 11329 (2019).
21. B. K. Shrewsbury, A. M. Morsy, and M. L. Povinelli, "Multilayer planar structure for optimized passive thermal homeostasis," Opt. Mater. Express **12**(4), 1442–1449 (2022).
22. M. Ono, K. Chen, W. Li, and S. Fan, "Self-adaptive radiative cooling based on phase change materials," Opt. Express **26**(18), A777–A787 (2018).
23. M. Ono, M. Takata, M. Shirata, T. Yoshihiro, T. Tani, M. Naya, and T. Saiki, "Self-adaptive control of infrared emissivity in a solution-processed plasmonic structure," Opt. Express **29**(22), 36048–36060 (2021).
24. H. Ji, D. Liu, H. Cheng, C. Zhang, and L. Yang, "Vanadium dioxide nanopowders with tunable emissivity for adaptive infrared camouflage in both thermal atmospheric windows," Sol. Energy Mater. Sol. Cells **175**, 96–101 (2018).
25. X. Wu, L. Yuan, X. Weng, L. Qi, B. Wei, and W. He, "Passive Smart Thermal Control Coatings Incorporating CaF_2/VO_2 Core–Shell Microsphere Structures," Nano Lett. **21**(9), 3908–3914 (2021).
26. M. Soltani and A. B. Kaye, "Properties and Applications of Thermochromic Vanadium Dioxide Smart Coatings," Intelligent Coatings for Corrosion Control, 461–490 (2015).

Optics EXPRESS

27. H. Wang, Y. Yang, and L. Wang, "Wavelength-tunable infrared metamaterial by tailoring magnetic resonance condition with VO_2 phase transition," J. Appl. Phys. **116**(12), 123503 (2014).
28. S.-H. Wu, M. Chen, M. T. Barako, V. Jankovic, P. W. Hon, L. A. Sweatlock, and M. L. Povinelli, "Thermal homeostasis using microstructured phase-change materials," Optica **4**(11), 1390–1396 (2017).
29. K. Sun, C. A. Riedel, A. Urbani, M. Simeoni, S. Mengali, M. Zalkovskij, B. Bilenberg, C. De Groot, and O. L. Muskens, "VO_2 thermochromic metamaterial-based smart optical solar reflector," ACS Photonics **5**(6), 2280–2286 (2018).
30. W. Zhang, H. Qi, A. Sun, Y. Ren, and J. Shi, "Periodic trapezoidal VO_2-Ge multilayer absorber for dynamic radiative cooling," Opt. Express **28**(14), 20609–20623 (2020).
31. A. M. Morsy, M. T. Barako, V. Jankovic, V. D. Wheeler, M. W. Knight, G. T. Papadakis, L. A. Sweatlock, P. W. Hon, and M. L. Povinelli, "Experimental demonstration of dynamic thermal regulation using vanadium dioxide thin films," Sci. Rep. **10**(1), 1–10 (2020).
32. C. Wan, Z. Zhang, D. Woolf, C. M. Hessel, J. Rensberg, J. M. Hensley, Y. Xiao, A. Shahsafi, J. Salman, and S. Richter, "On the optical properties of thin-film vanadium dioxide from the visible to the far infrared," Ann. Phys. **531**, 1900188 (2019).
33. D. Palik and Edward, *Handbook of optical constants of solids* (Academic press, 1985).
34. D. R. Lide, *handbook of chemistry and physics* (CRC Press, 1990).
35. M. A. Kats, D. Sharma, J. Lin, P. Genevet, R. Blanchard, Z. Yang, M. M. Qazilbash, D. Basov, S. Ramanathan, and F. Capasso, "Ultra-thin perfect absorber employing a tunable phase change material," Appl. Phys. Lett. **101**(22), 221101 (2012).
36. M. Moharam and T. Gaylord, "Rigorous coupled-wave analysis of planar-grating diffraction," J. Opt. Soc. Am. **71**(7), 811–818 (1981).
37. M. Moharam, E. B. Grann, D. A. Pommet, and T. Gaylord, "Formulation for stable and efficient implementation of the rigorous coupled-wave analysis of binary gratings," J. Opt. Soc. Am. A **12**(5), 1068–1076 (1995).
38. X. Fang, C. Zhao, and H. Bao, "Study on a novel selective solar absorber with surface ultrathin metal film," in *International Conference on Micro/Nanoscale Heat Transfer*, (American Society of Mechanical Engineers, 2016), V001T005A009.
39. A. Paone, R. Sanjines, P. Jeanneret, and A. Schüler, "Temperature-dependent multiangle FTIR NIR–MIR ellipsometry of thermochromic VO_2 and $V_{1-x}W_xO_2$ films," Sol. Energy **118**, 107–116 (2015).